The 9th European Congress on Computational Methods in Applied Sciences and Engineering
ECCOMAS Congress 2024
3–7 June 2024, Lisboa, Portugal

MRI-BASED COMPUTATIONAL MODELING OF HUMAN CORTICAL FOLDING

ANNE KERACHNI[1], THOMAS LAVIGNE[2,3,4], STEPHANE URCUN[2], MIREIA ALENYA[5], OSCAR CAMARA[5], JULIEN LEFEVRE[6], FRANÇOIS ROUSSEAU[1]

[1] IMT Atlantique, LaTIM U1101 INSERM, Brest, France

[2] Department of Engineering, Faculty of Science, Technology and Medicine, University of Luxembourg, Esch-sur-Alzette, Luxembourg

[3] Arts et Métiers Institute of Technology, IBHGC, Paris, France

[4] Arts et Métiers Institute of Technology, Univ. of Bordeaux, CNRS, Bordeaux INP, INRAE, I2M, UMR 5295, Talence, France

[5] BCN-MedTech, DTIC, Universitat Pompeu Fabra, Barcelona, Spain

[6] Aix Marseille Univ, CNRS, INT, Inst Neurosci Timone, Marseille, France

Key words: Brain development, Biomechanics, Growth, Cortical folding, Fetal magnetic resonance imaging

Summary. Multiple factors and scales are at play in the development of the human brain during gestation and especially in the emergence of cortical folds. Considering the complex interconnections between microstructure and mechanics can enrich our understanding of the main factors leading to human brain folding. Computational modeling is a promising way to explore the brain growth biomechanics. In this work, we investigate the use of anatomical and diffusion MRI data to inform the 3D computational model. The key contribution of this work lies in the joint use of a dynamical brain growth computational model and MRI-based features to simulate cortical folding. Cortical and inner layers are modeled as nearly-incompressible Neo-Hookean materials. The accurate delineation of the cortical layer is obtained from MRI data segmentation maps. The tangential cortical growth rate is defined as a spatio-temporal function of Fractional Anisotropy (FA), taken as a measure of neuronal maturation in the cortex. 3D brain folding simulations have been applied on realistic brain meshes, generated from segmented T2w MRI data. FA has been computed from diffusion MRI data using tensor based modeling. The results show that heterogeneous data-driven growth rate leads to significantly different folding patterns than using uniform pre-defined growth rate. The presented approach proposes to couple the mechanical deformation to the microstructural behavior of both cortical and inner layers via MRI data. It also opens to the use of specific parameters at voxel scale in 3D brain growth models.

1 INTRODUCTION

The developing human brain is smooth until the third trimester of pregnancy. At this time, convolutions begin to emerge on the surface of the cortex. They gradually develop to form a structured pattern of folds (gyri and sulci), at birth. Mechanical factors, more particularly deformations induced by a more intense growth in the cortex than in the inner layers of the brain, seem to be involved in this phenomenon [1, 2, 3, 4]. However, as highlighted by [5], cellular mechanisms at work remain uncertain. Computational models enable to explore the origins of the cortex morphogenesis. Purely mechanical (i.e. macroscopic) models have shown biophysical parameters such as growth rate, thickness of the cerebral cortex or respective stiffnesses of the cortex and sub-cortical layers strongly influence the simulated folding pattern [3, 6, 7, 8]. However, in reality, these parameters are neither homogeneous in space nor constant in time. [9] showed introducing a heterogeneous cortical thickness produces a less regular, more realistic folding pattern. In [10], the cortex presents a spatio-temporal gradient of expansion from the frontal/parietal regions which develops at the early ages of gestation (27 to 31 gestational weeks (GW)), to the parietal zone in the middle ages (31 to 33 GW) and finally to the frontal and temporal regions in late ages (33 to 37 GW). [11] correlated significantly the fractional anisotropy in four brain regions: the cortex, the corona radiata, the corpus callosum and the basal ganglia to their specific mechanical stiffness. More advanced models incorporate microstructural information, mimicking mechanobiological behaviors (reaction of cells to mechanical stresses) [12, 13], coupling cellular laws with the mechanical laws of the macroscopic continuum ("multi-field" or "coupled" models) [14, 5, 15]. All the previous examples raise the question whether a heterogeneous model informed by microstructural data could better reflect the emergence of brain folds. In this work, we use fetal MRI data from the developing Human Connectome Project (dHCP) [1] to inform our mechanical computational model. We simulate cortical folding on a 3D MRI-based brain geometry, as in [4, 16, 17]. Additionally, two key parameters of our model are informed with the data: the cortical thickness and the cortical growth ratio. First, we accurately delineate the cortical layer from MRI data segmentation maps. Second, we propose to consider Fractional Anisotropy (FA), computed from diffusion MRI data using tensor based modeling, as a spatio-temporal marker of the state of neuronal maturity in the cortex, and suppose that the growth rate depends on it. We finally assess the validity of the heterogeneous data-driven model by analyzing the induced curvature, and with a *Spangy* [18, 19] frequency band analysis to monitor the dynamics of the emergence of successive folds in the fetal cerebral cortex.

2 MATHEMATICAL MODEL OF BRAIN CORTEX FOLDING

2.1 Growth-induced irreversible deformations

2.1.1 A bilayer geometry: cortex and sub-layers

Cortex and inner layers are modeled as two distinguished materials with proper mechanical and growth properties. In particular, the main hypothesis behind biomechanical gyrification models is that the cortical layer grows more intensely than the inner layers [4].

[1] `https://gin.g-node.org/kcl_cdb/fetal_brain_mri_atlas`

2.1.2 Growth tensor: cortical, tangential and adaptative

During the morphogenesis of the human brain, neurons first migrate from inner layers to the cortex and then, neurons maturate in the cortex. Our model aims at representing the second phase, during which folds appear at the brain surface. In macroscopic computational models, neural maturation is represented by a growth tensor. We consider growth in cortex exclusively, which is traduced mathematically by introducing the weighting functions $\mathrm{gr}_{\mathrm{Cortex}}$ that cancel growth in the inner layers, as defined in Fig. 1 a. Additionally, we also introduce $\mathrm{gr}_{\mathrm{GrowthZones}}$ that cancels growth in the cortical regions shown in Fig. 3, so that only regions of interest grow. Then we assume cortex grows in the cortical surface plane (i.e. tangentially) [4], so the growth tensor is decomposed into tangential and radial compounds. Moreover, at each time step of the simulation, the local orientation of the cortical surface plane, through the normal vector $\mathrm{N_t}$, is recomputed to get an adaptative growth tensor, as explained in [13]. We finally consider the growth tensor of Eq. 1.

$$\underline{\underline{\mathrm{F}}}^{\mathrm{i}}_{\mathrm{g}} = (1 + \mathrm{gr}_{\mathrm{Cortex}}(\underline{\mathrm{X}}_{\mathrm{i}}) \cdot \mathrm{gr}_{\mathrm{GrowthZones}}(\underline{\mathrm{X}}_{\mathrm{i}}) \cdot \mathrm{dg}_{\mathrm{TAN}}) \cdot (\underline{\underline{\mathrm{I}}} - \underline{\mathrm{N}}_{\mathrm{t_i}} \otimes \underline{\mathrm{N}}_{\mathrm{t_i}}) + \underline{\mathrm{N}}_{\mathrm{t_i}} \otimes \underline{\mathrm{N}}_{\mathrm{t_i}} \tag{1}$$

We consider a linear variation of the growth such that:

$$\mathrm{dg}_{\mathrm{TAN}} = \alpha_{\mathrm{TAN}} \cdot \mathrm{dt}, \forall \mathrm{t} \tag{2}$$

2.1.3 Kinematics

We use multiplicative decomposition of the total deformation gradient. $\mathrm{F^g}$ is the irreversible growth part of the deformation from reference configuration to the intermediate stress-free configuration, $\mathrm{F^e}$ is the reversible elastic part of the deformation from the intermediate to the current configuration ([13]) and u is the unknown displacement field:

$$\underline{\underline{\mathrm{F}}} = \underline{\underline{\mathrm{F}}}^{\mathrm{e}} \cdot \underline{\underline{\mathrm{F}}}^{\mathrm{g}} \Rightarrow \underline{\underline{\mathrm{F}}}^{\mathrm{e}} = \underline{\underline{\mathrm{F}}} \cdot (\underline{\underline{\mathrm{F}}}^{\mathrm{g}})^{-1} = (\mathrm{Id} + \nabla_{\mathrm{X}} \underline{\mathrm{u}})(\underline{\underline{\mathrm{F}}}^{\mathrm{g}})^{-1} \tag{3}$$

2.2 Constitutive law: hyper-elasticity

We model cortex and inner layers as slightly compressible Neo-Hookean non-linear elastic materials, choosing the following strain energy density function:

$$\Psi(\underline{\underline{\mathrm{C}}}^{\mathrm{e}}, \mathrm{J^e}) = \frac{\mu}{2}(\mathrm{tr}(\underline{\underline{\mathrm{C}}}^{\mathrm{e}})\mathrm{J}^{\mathrm{e}-2/3} - 3) + \frac{\mathrm{K}}{2}(\mathrm{J^e} - 1)^2 \tag{4}$$

The elastic deformation gradient defined previously is used to build the right Cauchy-Green deformation tensor:

$$\underline{\underline{\mathrm{C}}}^{\mathrm{e}} = (\underline{\underline{\mathrm{F}}}^{\mathrm{e}})^{\mathrm{T}} \underline{\underline{\mathrm{F}}}^{\mathrm{e}} \tag{5}$$

and one of the principal invariants of $\underline{\underline{\mathrm{C}}}^{\mathrm{e}}$ tensor (of rank two) of dimension three:

$$\mathrm{J^e} = \det(\underline{\underline{\mathrm{F}}}^{\mathrm{e}}) \tag{6}$$

μ is the shear modulus. K the bulk modulus of the brain, computed from the Poisson ratio ν, with the Lamé coefficient relation $\mathrm{K} = \frac{2\ \mu\ (1+\nu)}{3\ (1-2\nu)}$.

2.3 Problem

2.3.1 Quasistatic approximation of the balance equation of the linear momentum

Strong formulation

As explained in [13], the quasistatic approximation of the motion equation can be assumed. Fetal brain cortex growth-induced deformations can then be represented by successive mechanical equilibrii without traction (See 2.3.2). The ODE in its Lagrangian formulation:

$$-\nabla \cdot \underline{\underline{P}} = \rho_t \underline{b}, \, \forall X \text{ in } \Omega_t \tag{7}$$

where P is the first Piola-Kirchhoff stress defined as $\frac{\partial \Psi}{\partial F}$, b is the body forces applied to the domain and Ω_t the spatial 3D domain.

Variational formulation

Let $\underline{v}$ belong to $V = H_0^1(\Omega_0)$, an Hilbert space. Find $u \in V$ such as for all $v \in V$:

$$\int_{\Omega_t} \underline{\underline{P}} : \nabla \underline{v} \, dx = \int_{\Omega_t} \rho_t \underline{b} \cdot \underline{v} \, dx + \int_{\delta\Omega_t} \underline{N_t} \cdot \underline{\underline{P}} \cdot \underline{v} \, ds \tag{8}$$

with $\underline{N_t}$ the unit normal in the updated reference configuration, at the external surface of the brain (pial surface).

We neglect external body forces: $\rho_t \underline{b} \cdot \underline{v} \, dx = 0$. Among all abstract test functions $\underline{v}$, we choose the arbitrary test displacement field ∂u.

2.3.2 Boundaries and boundary conditions

$$\int_{\delta\Omega_t} \underline{N_t} \cdot \underline{\underline{P}} \cdot \underline{\partial u} \, ds = \int_{\Gamma_c^1} \underline{N_t} \cdot \underline{\underline{P}} \cdot \underline{\partial u} \, ds + \int_{\Gamma_c^2} \underline{N_t} \cdot \underline{\underline{P}} \cdot \underline{\partial u} \, ds + \int_{\Gamma_f} \underline{P_n} \cdot \underline{\partial u} \, ds + \int_{\Gamma_u} \underline{N_t} \cdot \underline{\underline{P}}(u_D) \cdot \underline{\partial u} \, ds \tag{9}$$

as detailed in [20], where Γ_c^1 is the contact boundary on the Left hemisphere; Γ_c^2 the contact boundary on the Right hemisphere; Γ_f the boundary where Neumann conditions apply ; Γ_u the boundary where Dirichlet conditions apply.

The traction part $\int_{\Gamma_f} \underline{P_n} \cdot \underline{\partial u} \, ds$ is considered null.

Unilateral contact of each hemisphere against fictive interhemispheric rigid planes

Two types of collisions appear during the brain folding simulations: self-contact between the two hemispheres and then, self-contact between the emerging folds themselves. We only model the contact between the two hemispheres. To do so, two fictive interhemispheric planes are introduced, against which each hemisphere is going to collide, as shown in Fig. 1 b.

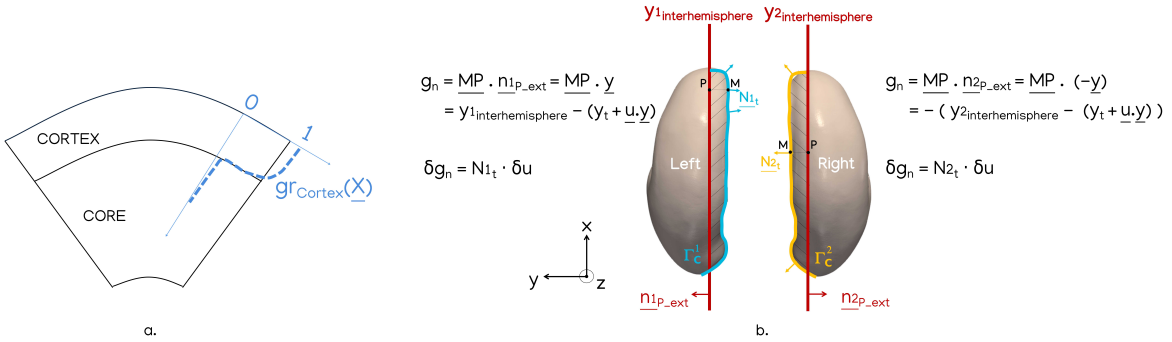

Figure 1: a. gr_{Cortex} b. Penalty method to avoid collision between the Left and Right hemispheres, introducing two interhemispheric planes

For each hemisphere, the contact is avoided using the penalty method [20].
Considering all the previous hypotheses, (8) becomes:

$$\int_{\Omega_t} \underline{\underline{P}}(u) : \nabla \underline{\partial u}\, dx \; + \int_{\Gamma_c^1 \cup \Gamma_c^2} \varepsilon \; < g_n > \; \delta g_n \, ds \; = \int_{\Gamma_u} \underline{N_t} \cdot \underline{\underline{P}}(u_D) \cdot \underline{\partial u}\, ds \tag{10}$$

where g_n is the normal gap between a surface node of one hemisphere and the plane, δg_n the virtual penetration, detailed in Fig. 1 b. and ε the penalty coefficient. $< g_n >= g_n$ if $g_n \geq 0$ (contact) and $< g_n >= 0$ if $g_n < 0$ (separation).

3 CONTRIBUTION OF MRI DATA IN MULTI-SCALE MODELING OF BRAIN GROWTH

3.1 Fetal MRI atlas data from the dHCP project

The dHCP project notably provides a multi-modal atlas of volumetric fetal magnetic resonance images from 21 to 36GW. We use T2 weighted (T2w) data; the segmentations providing labels to different brain regions; the fractional anisotropy (FA) data and the affine transformations enabling to obtain the mapping between the image space and the world coordinate space. MRI data are used both to generate the brain geometry and MRI-informed cortex delineation and growth rate, as shown in Fig.2.

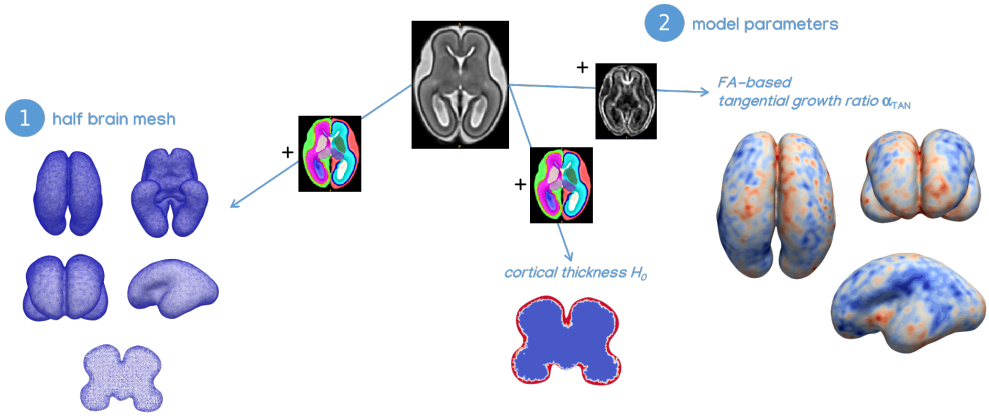

Figure 2: MRI data contribute to both the geometry generation, H_0 and α_{TAN} parameters definition.

3.2 Generation of a realistic brain geometry

The affine transformation is first applied to the T2w data at 21GW, as well as to the associated parcellation (and FA) maps at 21 GW. We mask the T2w images using the labels of interest to only keep regions located beneath the cerebral cortex. Then, the cortex contour on the masked T2w is segmented with *3D Slicer* [2], smoothed and a 2D surface brain mesh is generated and exported (.stl). The quality of the 2D brain mesh is then improved using *Meshlab* [3]. The 3D tetrahedral brain mesh is generated with *Netgen* [4] and finally, the mesh is converted into .xmdf/.h5 format and refined near by the surface.

3.3 Delineation of the cortex layer H_0 from MRI parcellation

The segmentation labels from the input image (image space) are interpolated over all mesh nodes (world coordinates space), thanks to the affine transformation. The nearest neighbour interpolation method is used. We then transform the segmentation labeling from the dHCP into a binary labeling, allocating 1 to the nodes in the cortex and 0 otherwise, as shown in Fig. 2.

3.4 FA-based tangential growth ratio

3.4.1 Fractional Anisotropy, neuronal maturation in the cortex and cortical folding

FA is an index between 0 and 1, obtained from Diffusion-weighted magnetic resonance imaging (diffusion MRI), using tensor based modeling (DTI). In the cortex, it reflects the presence of a privileged orientation of the local neural cortical connections (axons and dendrites). [21, 22] show the cortical folding phase coincides with a decrease in FA over gestational time; FA is correlated with curvature [22, 23]. According to [24], during the migration period, the radial organization persists more under the gyri than under the sulci. On the other hand, radial organization does not necessarily mean higher FA. Moreover, in more than half of the ferret brains data analyzed in [22], the FA is higher in the sulci. As well, [25] shows that the density of the fibers is greater under the gyri. On the FA projections that we made on the dHCP meshes, we can see at 28GW, FA is weaker around the central sulcus area, where the growth is supposed to be relatively high, according to [10]. Finally, [23] found correlation between FA and curvature or between their variations, but not between FA and cortical surface expansion nor between their variations. In this work, we use modelling to test a potential correlation between FA and the variation of cortical expansion rate.

3.4.2 FA-based tangential growth ratio α_{TAN}

The FA values at 21GW from the input image (image space) are interpolated over all mesh nodes (world coordinates space), thanks to the affine transformation, using the linear method. To get the FA-based cortical growth rate, the FA is first normalized.

We have tested various correlation laws and finally assume a relatively low FA value in the cortex, meaning no privileged orientation of the microstructure, is associated with a relatively fast growth rate. We consider three different tangential growth rate to test in the

[2] `https://www.slicer.org/`

[3] `www.meshlab.net`

[4] `https://ngsolve.org/`

model: a homogeneous growth rate (4.2); a growth rate correlated spatially with FA, defined by $\alpha\mathrm{TAN}_{\mathrm{FA}}(\underline{x}) = \beta/(1+\mathrm{FA}(\underline{x}, \mathrm{T}_0))$ and a growth rate correlated in space and time with FA defined by $\alpha\mathrm{TAN}_{\mathrm{FA}}(\underline{x}, t) = \beta/(1 + \mathrm{FA}(\underline{x}, \mathrm{T}_0)e^{-(t-\mathrm{T}_0)/\tau})$, where $\tau = 7$GW [26], $\mathrm{T}_0 = 21$GW and FA the normalized fractional anisotropy. The coefficient $\beta > 0$ enables to keep the growth intensity in the cortex comparable between the homogeneous model and the FA-based model, such that the integration over the cortex volume of the FA-based growth rate equals the one of the homogeneous growth rate $\alpha\mathrm{TAN}_{\mathrm{homogeneous}}$, i.e. $\int_{\mathrm{Cortex}} \alpha\mathrm{TAN}_{\mathrm{FA}}\, dx = \int_{\mathrm{Cortex}} \alpha\mathrm{TAN}_{\mathrm{homogeneous}}\, dx$.

β is computed in each case of a FA-based growth rate as $\dfrac{\mathrm{N}_{\mathrm{Cortex}} \cdot \alpha\mathrm{TAN}_{\mathrm{homogeneous}}}{(\sum_{\mathrm{i}}^{\mathrm{N}_{\mathrm{Cortex}}} \alpha\mathrm{TAN}_{\mathrm{FA}})}$.

4 COMPUTATIONAL MODEL, SIMULATIONS AND RESULTS

4.1 Computational model

We developed the *braingrowthFEniCS* computational model [5] with the open-source FEniCS library [27], to simulate cortical folding. The MRI-based brain spatial domain is illustrated in Fig. 2 1. and discretized by 147917 vertices, 719399 tetrahedral elements and 106112 surface triangle elements. Brain areas that are not supposed to grow (e.g. the longitudinal fissure, the ventricles, and the mammilary bodies) are defined. The boundaries entities are marked to then define the boundary conditions, as shown in Fig. 3. The growing boundary is traction-free. The non-growing boundaries are fully fixed to prevent rotations and translations to be included in the problem solution. A band is chosen to define the zone where contact between the two hemispheres should occur. Then the surface is marked within this contact zone for both the Left and Right hemispheres. At each iteration, the problem is linearized using a *Newton-Raphson* solver with absolute tolerance: 10^{-9} ($\mathrm{N.m}^{-3}$), relative tolerance: 10^{-6} and max iterations: 10. The direct solver *mumps* is then used (on single processor) to solve the linearized problem.

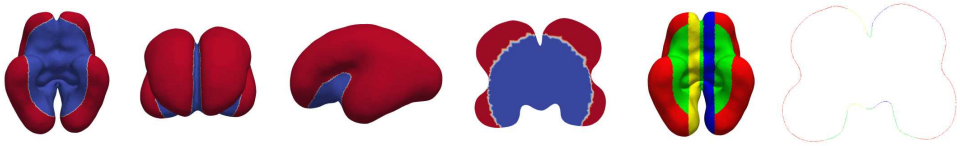

Figure 3: The four first figures show the $\mathrm{gr}_{\mathrm{GrowthZones}}$ weighting function (red: 1; blue: 0), defined to avoid the blue regions to grow. The two last the boundaries: Dirichlet boundary conditions where brain is not growing (green), contact boundaries for the Left hemisphere (yellow) and the Right hemisphere (blue).

4.2 Biophysical model parameters

Model parameters, expressed in the international system unit and based on physical experiments offer reliable and interpretable simulation results [28, 29]. This also enables to compare simulation results with real data, at the corresponding time point. In this vain, the initial MRI-based brain geometry was converted into meters. When homogeneous, the cortical thickness H_0 was set at $1.8 \cdot 10^{-3}$ m [30, 31]; the shear modulus in cortex μ_{Cortex} at 450 Pa; the shear modulus in inner layers μ_{Core} at 150 Pa (preserving the stiffnesses ratio from [3, 32]) and the Poisson ratio at 0.45 [4]. For the homogeneous tangential growth rate, we estimated its value as a variation of elongation over time variation, computed it from the cortical areas at 21 and 36 GW and

[5] `https://github.com/annekerachni/braingrowthFEniCS/`

obtained α_{TAN} equal to $2.0 \cdot 10^{-7}$ (m).s^{-1}; the penalty coefficient was set empirically at ε equal to $5.0 \cdot 10^{5}$; initial simulation time T_0 at 21 GW; maximum simulation time T_{max} at 36 GW and time-step dt at 43200 seconds.

4.3 Simulations

Brain growth is simulated from 21GW, both considering an homogeneous cortical thickness (see value in 4.2) and a MRI-based cortical thickness (3.3). Within those two cases, the three different tangential growth rates detailed in 3.4.2 are tested. One simulation from 21 to 28GW takes $\sim$ 15 hours ($\sim$ 2 hours per gestational week) on Intel Xeon mono-cpu.

4.4 Results

About reproducing the consistent folds in the fetal brain across individuals (primary folds)

[33] showed both consistency and variability in the folding pattern of two developing brains. In particular, the *central sulcus* and *intraparietal sulcus* are likely to be commonly located. [34] proposed a review of gestational times of emergence of sulci, with the first emerging folds: around 22-23 GW, the *calcarine sulcus*, the *posterior* and *anterior cingulate sulcus*; then, around 24-25 GW, the *central sulcus*, separating the frontal and the parietal lobes, the *collateral sulcus* and the *superior frontal sulcus*.

Folds emergence on simulation and on the dHCP data

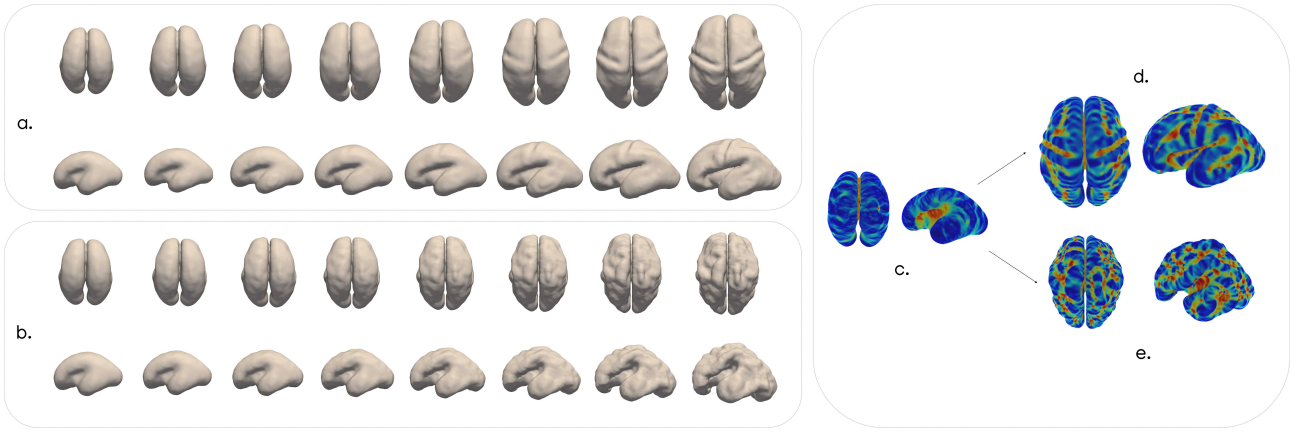

Figure 4: Dynamics of cortical folding from 21 to 28 GW for the dHCP data (a.) and for simulation with growth rate $\alpha TAN_{FA}(\underline{x}, t) = \beta/(1+FA(\underline{x}, T_0)e^{-(t-T_0)/\tau})$ and H0 from MRI segmentation (b.). Shape index computed for initial smooth dHCP mesh at 21GW (c.) and both dHCP mesh (d.) and simulation (e.) at 28GW.

Fig. 4 a. and b. show our simulations can reproduce folding, but do not reproduce the emergence of one of the first fold, namely the central sulcus. This can be due to the initial smooth mesh which probably already presents irregularities emphasized during the growth. The impact of the model parameters also needs to be explored further. Additionally, the simulation volumes are less inflated than the real data ones, and some hypothesis, like growth in the inner layers, could be added to the model.

Frequency band analysis (Spangy)

We want to know to what extend the simulation results obtained with the *braingrowthFEniCS*

model are able to represent the emergence of the primary folds. To do so, we carry out a spectral analysis by band with the *Spangy* method [6] to compare the folding dynamics of the simulations with those shown by the dHCP data.
Spangy decomposes a folding proxy (e.g. curvature, shape index) defined on the cerebral cortex surface mesh on the basis of modes of the Laplace-Beltrami operator, and decomposes the spectrum into spatial frequency bands. The spectral density and relative spectral density (to the total spectral density) are computed for each frequency band. Depending on the local value of the proxy, the cortical surface is associated with a dominant band of spatial frequencies (B_{-6} to B_6). As spatial frequency bands B_4, B_5 and B_6 could be associated respectively with the primary, secondary and tertiary folds appearing successively during brain development, this metric is used to characterize and compare the folding dynamics of both the simulations and the dHCP data [18, 19]. The *shape index*, a decomposition of the curvature [35] between -1 and 1, is the proxy chosen (See shape index computed for dHCP and simulation meshes in Fig. 4 c., d. and e.). It characterizes the local shape of a surface. As mentioned in [36], it is independent to the brain mesh size, unlike curvature.

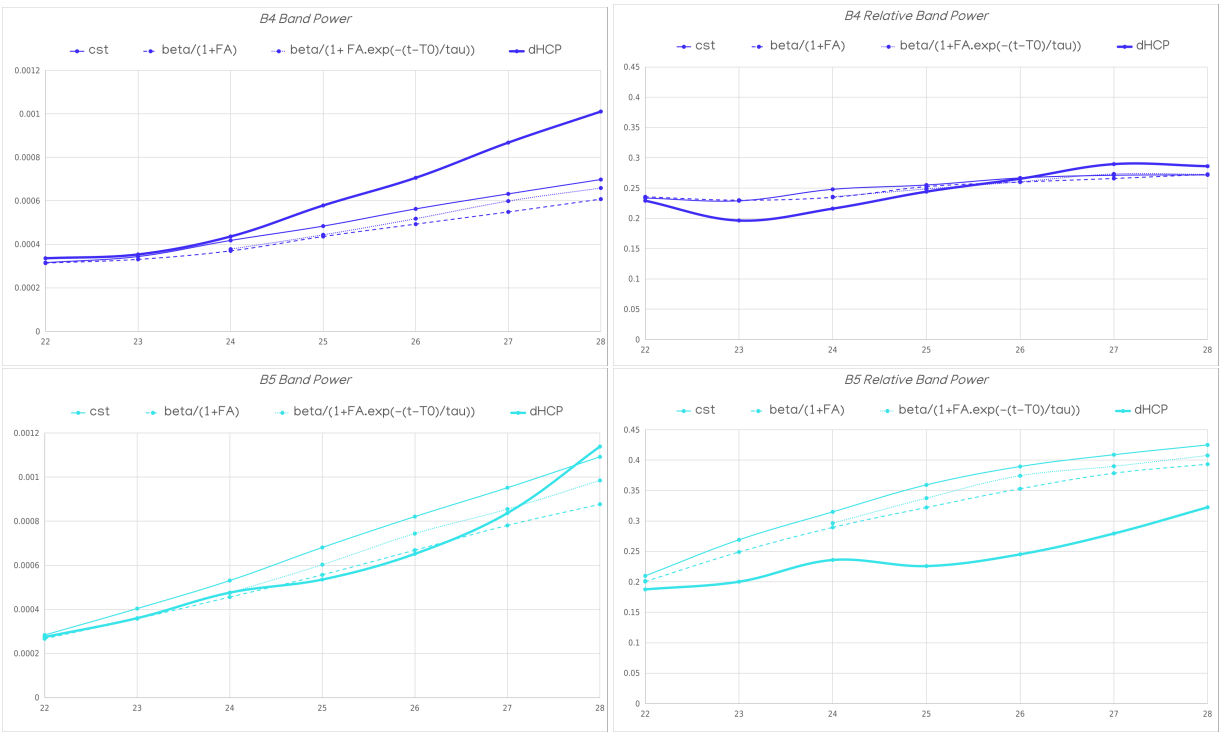

Figure 5: Evolution of the spectral density associated with frequency bands B4 and B5 for simulations with H0 constant and the three tangential growth rates, and for the dHCP data. Relative Band Power is the spectral power normalized to total spectral power.

[6] `https://github.com/gauzias/slam/blob/master/slam/spangy.py`

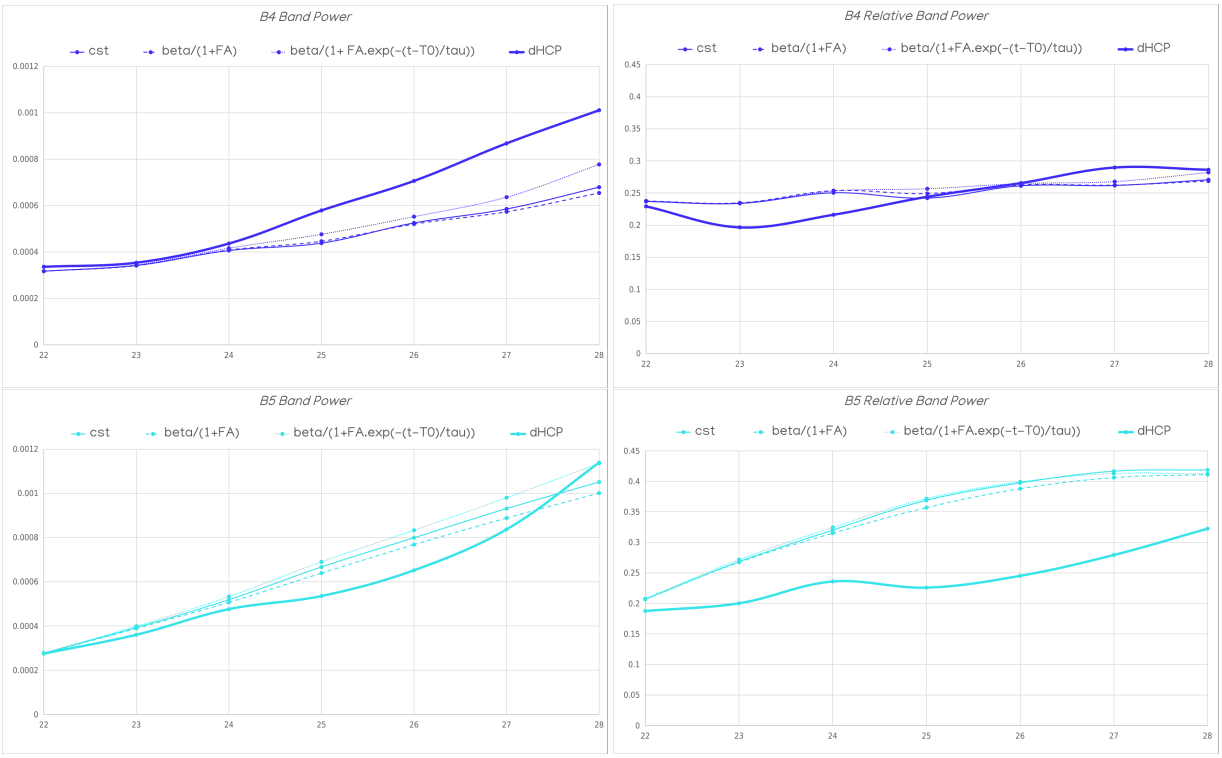

Figure 6: Evolution of the spectral density associated with frequency bands B4 and B5 for the simulations with H0 from MRI segmentation and the three tangential growth rates, and for the dHCP data.

Fig. 5 and 6 show the spectrum associated to shape index of the cortical surface are relatively more regular for simulations than for the dHCP data. Then, from 25GW when the first folds emerge, B4 frequencies are slightly less represented in all the simulations compared to the real data (this observation can be nuanced when considering B4 relative band power that is comparable between simulations and dHCP), while B5 frequencies seem too represented, meaning our model probably favors high frequency folds at the expense of primary ones. It can be also seen qualitatively on the folded meshes from the simulations. The simulations with MRI-based segmentation appear, in our case, further from the real data fold shape spectrum.
In terms of the impact of using a FA-based growth rate, the simulations with a constant tangential growth rate seem to globally better approximate the dHCP data for B4 frequencies from 25GW (H0 homogeneous), while the simulations with a growth rate spatially correlated with FA are closer to the real data for relative B5 frequencies.

5 CONCLUSION

We use fetal MRI data to incorporate heterogeneity into the parameters of our brain growth model. In particular, we propose to correlate the fractional anisotropy data with the cortical growth rate and to quantify the impact on the type of folds obtained, via a frequency band analysis based on the shape index proxy. Our simulations with a FA-based growth rate, compared to the one with an homogeneous one, show the growth law responsible for the emergence of primary folds (B4) does not seem to be the same as the one for secondary folds (B5). This

work allows to consider incorporating data from medical imaging to investigate the link between macroscopic deformation and the microstructural behavior and the impact of their entanglement onto the human cortical folding pattern. A further calibration of the model is to be done to better approximate the morphology of the real data and a growth law may be defined from the longitudinal FA maps.

References

[1] D.P. Richman et al. "Mechanical model of brain convolutional development". In: *Science* 189 (1975), pp. 18–21.

[2] L. Ronan et al. "Differential tangential expansion as a mechanism for cortical gyrification". In: *Cereb. Cortex* (2013).

[3] S. Budday et al. "A mechanical model predicts morphological abnormalities in the developing human brain". In: *Scientific reports* 4.1 (1975), p. 5644.

[4] T. Tallinen et al. "On the growth and form of cortical convolutions". In: *Nature Physics* 12.6 (2016), pp. 588–593.

[5] M.S. Zarzor et al. "A two-field computational model couples cellular brain development with cortical folding". In: *Brain Multiphysics* 2 (2021), p. 100025.

[6] P.V. Bayly et al. "A cortical folding model incorporating stress-dependent growth explains gyral wavelengths and stress patterns in the developing brain." In: *Physical biology* 10.1 (2013), p. 016005.

[7] M.A. Holland et al. "Emerging brain morphologies from axonal elongation". In: *Annals of biomedical engineering* 43 (2015), pp. 1640–1653.

[8] X. Wang et al. "The influence of biophysical parameters in a biomechanical model of cortical folding patterns". In: *Scientific Reports* 11.1 (2021), p. 7686.

[9] L. da C. Campos et al. "The role of thickness inhomogeneities in hierarchical cortical folding". In: *Cond-Mat Physics Q-Bio* (2020).

[10] K.E. Garcia et al. "Dynamic patterns of cortical expansion during folding of the preterm human brain". In: *Proceedings of the National Academy of Sciences* 115.12 (2018), pp. 3156–3161.

[11] S. Budday et al. "Mechanical characterization of human brain tissue". In: *Acta biomaterialia* 48 (2017), pp. 319–340.

[12] S. Budday and P. Steinmann. "On the influence of inhomogeneous stiffness and growth on mechanical instabilities in the developing brain". In: *International Journal of Solids and Structures* 132 (2018), pp. 31–41.

[13] S. Wang et al. "Numerical investigation of biomechanically coupled growth in cortical folding". In: *Biomechanics and Modeling in Mechanobiology* 20.2 (2021), pp. 555–567.

[14] R. de Rooij and E. Kuhl. "A physical multifield model predicts the development of volume and structure in the human brain". In: *Journal of the Mechanics and Physics of Solids* 112 (2018), pp. 563–576.

[15] M.S. Zarzor et al. "Exploring the role of the outer subventricular zone during cortical folding through a physics-based model". In: *elife* 12 (2023), e82925.

[16] M. Alenyà et al. "Computational pipeline for the generation and validation of patient-specific mechanical models of brain development." In: *Brain Multiphysics* 3 (2022), p. 100045.

[17] Z. Wang et al. "An inverse modelling study on the local volume changes during early morphoelastic growth of the fetal human brain". In: *Brain multiphysics* 2 (2021), p. 100023.
[18] D. Germanaud et al. "Larger is twistier : spectral analysis of gyrification (SPANGY) applied to adult brain size polymorphism". In: *NeuroImage* 63.3 (2012), pp. 1257–1272.
[19] J. Dubois et al. "The dynamics of cortical folding waves and prematurity-related deviations revealed by spatial and spectral analysis of gyrification". In: *NeuroImage* 185 (2019), pp. 934–946.
[20] Vladislav A. Yastrebov. *Numerical methods in contact mechanics*. John Wiley & Sons, 2013, pp. 151–155.
[21] M. Ouyang et al. "Delineation of early brain development from fetuses to infants with diffusion MRI and beyond". In: *Neuroimage* 185 (2019), pp. 836–850.
[22] C.D. Kroenke et al. "Regional patterns of cerebral cortical differentiation determined by diffusion tensor MRI". In: *Cerebral Cortex* 19.12 (2009), pp. 2916–2929.
[23] X. Wang et al. "Folding, but not surface area expansion, is associated with cellular morphological maturation in the fetal cerebral cortex". In: *Journal of Neuroscience* 37.8 (2017), pp. 1971–1983.
[24] E. Takahashi et al. "Emerging cerebral connectivity in the human fetal brain: an MR tractography study". In: *Cerebral cortex* 22.2 (2012), pp. 455–464.
[25] P. Chavoshnejad et al. "Role of axonal fibers in the cortical folding patterns: A tale of variability and regularity". In: *Brain Multiphysics* 2 (2021), p. 100029.
[26] Kroenke C.D. "Using diffusion anisotropy to study cerebral cortical gray matter development". In: *Journal of Magnetic Resonance* 292 (2018), pp. 106–116.
[27] M.S. Alnaes et al. "The FEniCS project version 1.5". In: *Archive of Numerical Software* 3 (2015).
[28] S. Urcun et al. "Non-operable glioblastoma: proposition of patient-specific forecasting by image-informed poromechanical model". In: *Brain Multiphysics* 4 (2023), p. 100067.
[29] T. Lavigne et al. "Single and bi-compartment poro-elastic model of perfused biological soft tissues: FEniCSx implementation and tutorial". In: *Journal of the Mechanical Behavior of Biomedical Materials* 143 (2023), p. 105902.
[30] J. Wu et al. "Age-specific structural fetal brain atlases construction and cortical development quantification for chinese population". In: *Neuroimage* 241 (2021), p. 118412.
[31] F. Wang et al. "Developmental topography of cortical thickness during infancy". In: *Proceedings of the National Academy of Sciences* 116.32 (2019), pp. 15855–15860.
[32] M.J. Razavi et al. "Role of mechanical factors in cortical folding development". In: *Physical Review E* 92.3 (2015), p. 032701.
[33] N. Demirci et al. "Consistency and variation in the placement of cortical folds: a perspective". In: *Brain Multiphysics* 5 (2023), p. 100080.
[34] H. de Vareilles et al. "Development of cortical folds in the human brain: An attempt to review biological hypotheses, early neuroimaging investigations and functional correlates". In: *Developmental cognitive neuroscience* 61 (2023), p. 101249.
[35] J.J. Koenderink and A.J. Van Doorn. "Surface shape and curvature scales". In: *Image and vision computing* 10.8 (1992), pp. 557–564.
[36] N. Demirci et al. "Scaling patterns of cortical folding and thickness in early human brain development in comparison with primates". In: *Cerebral Cortex* 34.2 (2024), bhad462.